Driven kink in the Frenkel-Kontorova model

O. M. Braun,[1,2,*] Bambi Hu,[2,3] and A. Zeltser[2,4]
[1]*Institute of Physics, National Ukrainian Academy of Sciences, 03650 Kiev, Ukraine*
[2]*Department of Physics and CNS, Hong Kong Baptist University, Hong Kong, China*
[3]*Department of Physics, University of Houston, Houston, Texas 77204*
[4]*Physical-Technical Institute, National Ukrainian Academy of Sciences, UA-340114 Donetsk, Ukraine*
(Received 20 December 1999)

The dynamics of dc driven chain of harmonically interacting atoms in the external sinusoidal potential (the Frenkel-Kontorova model) is studied. It is shown that in the underdamped case the motion of the topological soliton (kink) becomes unstable at a high velocity due to excitation of the localized intrinsic kink mode (the discrete shape mode, or discrete breather) in the kink tail. When the amplitude of the breather's oscillation becomes large enough, it decays into a kink-antikink pair. The subsequent collision of newly created kink and antikink leads to a sharp transition to the running state, where all atoms of the chain slide over the external potential almost freely.

PACS number(s): 45.05.+x, 82.20.Mj, 63.20.Ry, 05.60.−k

I. INTRODUCTION

Driven dynamics of a system of interacting atoms is an interesting physical problem as well as it has important applications in mass and charge transport phenomena in solids and on crystal surfaces. One of important applications of driven dynamics has recently emerged in tribology studies, where a thin atomic layer is confined between two substrates which move with respect to one another (e.g., see [1] and references therein). Large-scale molecular dynamics simulation showed that this system exhibits a stick-slip motion on an atomic scale, which is explained by a sharp (first-order) transition of atoms in the confined layer from a ''locked'' state to the ''running'' state when the force applied to the upper substrate (or its velocity) increases over some threshold value. In the running state the atoms in the layer slide over the substrates almost freely, so the effective frictional force is small. If then the applied force decreases, the back transition to the locked state takes place at a smaller force, so the system exhibits hysteresis.

Such a behavior was observed in almost all systems studied: in three dimensional (3D) systems with realistic interatomic interaction [1,2], in the isotropic two dimensional (2D) system [3,4], in the anisotropic 2D system [5], in the one dimensional (1D) system with anharmonic (exponential) interaction [6], and in the classical Frenkel-Kontorova (FK) model [7,8], where the interatomic interaction is harmonic and the external potential is taken to be sinusoidal. Moreover, the hysteresis persists at nonzero temperatures [1–6].

A possible explanation of the hysteretic behavior may be done analogously to first-order phase transitions in thermodynamics: when the velocity of upper substrate increases, the temperature of confined layer may increase as well, so it has to melt finally, and this results in decreasing friction. However, it is hard to expect that the first-order phase transition exists in 1D systems, especially with repulsive interactions as was observed in [6]. Therefore, it was proposed [6] that the sharp transition to the running state has a solely dynamical origin.

Indeed, the system of interacting atoms subjected to the periodic substrate potential has the degenerated ground state, and the mass or charge transport in the system is carried out by topological defects, the local compression or expansion of the system (e.g., see [9]). These defects are known as kinks in the 1D FK model, and as domain walls or dislocations in 2D or 3D systems. However, these topological excitations usually cannot propagate with velocities higher than the sound speed. Thus, if one applies an external driving to accelerate the kink to a high enough velocity, its motion may become unstable and could result in a sharp transition to the running state. This scenario was observed in the simulation [6]. The goal of the present work is to study this phenomenon in detail and to clarify the mechanism of instability of fast topological excitations.

We consider the classical FK model with harmonic interaction and sinusoidal substrate potential at zero temperature. Compared with the classical FK model (e.g., see [9]), the new issues of the model under consideration are the following: we applied a dc force f to all atoms, and we assume also the external viscous damping with a coefficient η, so the motion equation is

$$\ddot{x}_l + \eta\dot{x}_l - g[x_{l+1} + x_{l-1} - 2x_l] + \sin x_l - f = 0, \qquad (1)$$

where x_l is the coordinate of lth atom and g is the elastic constant of harmonic interaction between nearest-neighbor atoms. Throughout the paper we use the dimensionless system of units, where the atomic mass is $m=1$, the period of the external potential is $a=2\pi$, and its amplitude is $\varepsilon=2$. In these units, a characteristic frequency of atomic vibration at the minimum of external potential is $\omega_0=1$, a characteristic time scale is $\tau_0=2\pi$, and the maximum value of the external dc force, when the minima of sinusoidal substrate potential disappear and topological excitations cannot exist anymore, is $f=1$. We use periodic boundary conditions with the number of atoms $N=N_s+1$, where N_s is the number of wells of the periodic potential, so we have one kink (excessive atom) inserted into the commensurate structure.

*Electronic address: obraun@iop.kiev.ua

The FK model as well as its generalizations were studied in a number of papers (e.g., see [9] and references therein). Without the external periodic potential the only excitations of the model are acoustic phonons with the spectrum $\omega_{\rm ph}(k)=ck$, where $c=2\pi\sqrt{g}$ is the sound velocity. However, with the presence of the external potential the spectrum becomes optical

$$\omega_{\rm ph}^2(k)=\omega_{\rm min}^2+2g(1-\cos 2\pi k), \tag{2}$$

where $\omega_{\rm min}^2=(1-f^2)^{1/2}$ and the wave vector k must belong to the first Brillouen zone, $|k|<1/2$, so the phonon frequencies lie within the interval $\omega_{\rm min}\leqslant\omega_{\rm ph}(k)\leqslant\omega_{\rm max}$, where $\omega_{\rm max}^2=\omega_{\rm min}^2+4g$. Besides, the FK model is nonlinear and admits two more kinds of excitations, the topological excitations called kinks and antikinks (they describe a local compression or extension of the chain respectively), and also the dynamical nonlinear excitations called discrete breathers (e.g., see [9]). The kinks are responsible for the dc mobility in the FK chain. In the continuum limit approximation, which can be used at large values of the elastic constant, $g\gg 1$, the motion equation (1) reduces to the well-known sine-Gordon (SG) equation, and the kinks move freely along the system. In the discrete system the kink motion is not free, the kink must overcome some potential barriers known as the Peierls-Nabarro (PN) barriers, so the kink starts to move only if the dc force exceeds some threshold value $f_{\rm PN}$. Besides, at least in the anticontinuum limit (i.e., when $g\ll 1$) the FK model supports the existence of localized nonlinear excitations, the so-called discrete breathers (DBs), which do not carry mass along the chain, but at a high amplitude of their vibration they may decay into a kink-antikink pair. These newly created kinks and antikinks then move independently and thus increase the system mobility. As will be shown in the present paper, namely the excitation of a discrete breather at the tail of moving kink is responsible for the instability of fast kink.

One more issue of the FK model is the existence of linear excitations of the kink itself, the so-called shape (internal) kink modes. Namely, if one looks for a solution of the motion equation in the form $x_l(t)=x_l^{(\rm kink)}+\psi_l(t)$ and then linearizes the resulting equation for ψ, it may have localized solutions that describe small-amplitude oscillations of the kink shape. In the exactly integrable SG equation the only mode of this type is the zero-frequency Goldstone mode, which describes the translational invariance of the SG equation. In the discrete FK model, such a mode also always exists, but now it has a nonzero frequency $\Omega_{\rm PN}<\omega_{\rm min}$, which corresponds to the kink's oscillation in the minimum of the PN potential. However, when the model deviates from the exactly integrable one, so that the kink shape deviates from the SG form, there may appear additional shape modes, either the low-frequency shape modes below the phonon spectrum, or/and the high-frequency modes above the phonon spectrum of the discrete chain. Namely, the additional shape modes may appear due to deviation of the substrate potential from the sinusoidal form (e.g., see [9,10] and references therein), due to anharmonicity of the interatomic interaction [11], and even solely due to discreteness effects [10]. Because the dc driving force f also leads to a change of the kink's shape, one may expect an appearance of shape modes for the driven kink as well. The shape modes are spatially localized objects with frequencies outside the phonon spectrum and, therefore, they correspond to long-living excitations of the system. This defines the importance of shape modes in system dynamics: for example, they may temporarily store energy at kinks' collisions. The shape mode can be treated as a discrete breather captured by the kink as was described in [12]. The essential difference of the captured discrete breather from the free one is that due to the kink, the captured breather is a linearly stable excitation, while the free discrete breather needs a nonzero threshold energy to be excited.

The paper is organized as follows. In Sec. II we study the driven model in the continuum limit approximation. Then in Sec. III we present the simulation results for the discrete chain. Finally, Sec. IV concludes the paper.

II. CONTINUUM LIMIT APPROXIMATION

For a large value of the elastic constant, $g\gg 1$, we can use the continuum limit approximation, $x_l(t)=2\pi l+u_l(t)$, $l\to x=2\pi l$, $u_l(t)\to u(x,t)$, $u_{l+1}(t)+u_{l-1}(t)-2u_l(t)\to(2\pi)^2u''(x,t)$, so that the motion equation (1) reduces to the form

$$\ddot{u}(x,t)+\eta\dot{u}(x,t)-d^2u''(x,t)+\sin u(x,t)-f=0, \tag{3}$$

where $d=2\pi\sqrt{g}$ is the width of the static kink (in our system of units $d=c$). For the case of $f=0$ and $\eta=0$, Eq. (3) reduces to the SG equation,

$$\ddot{u}(x,t)-d^2u''(x,t)+\sin u(x,t)=0. \tag{4}$$

The kink (excessive atom) solution of Eq. (4) has the form

$$u(x,t)=4\tan^{-1}\exp[-(x-vt)/d_k(v)]. \tag{5}$$

The SG kink, Eq. (5) can move with any velocity $|v|<c$ and is characterized by the width $d_k(v)=d(1-v^2/c^2)^{1/2}$ and the effective mass $m_k(v)=(4/\pi d)(1-v^2/c^2)^{-1/2}$.

Considering the kink of Eq. (3) as a stable quasiparticle and assuming that its parameters at nonzero f and η are the same as those of the SG kink, the steady-state kink velocity can be found approximately from the equation $v_k=f/\eta m_k(v_k)$ that leads to the dependence

$$v_k^{(\rm SG)}(f)=c\frac{\pi f}{\sqrt{(\pi f)^2+(4\eta)^2}}. \tag{6}$$

The dependence, Eq. (6), is shown in Fig. 1 by the dotted curve.

A general solution of Eq. (3) can be found numerically only. Looking for a steady-state solution in the form $u(x,t)=u_k(x-vt)$, we obtain for the function $u_k(z)$ the ordinary differential equation

$$(c^2-v^2)u_k''(z)+\eta v u_k'(z)-\sin u_k(z)+f=0. \tag{7}$$

Introducing the new variables $\xi=u_k(z)$ and $w(\xi)=u_k'(z)$, Eq. (7) reduces to the first-order differential equation

$$(c^2-v^2)w'(\xi)w(\xi)+\eta v w(\xi)-\sin\xi+f=0. \tag{8}$$

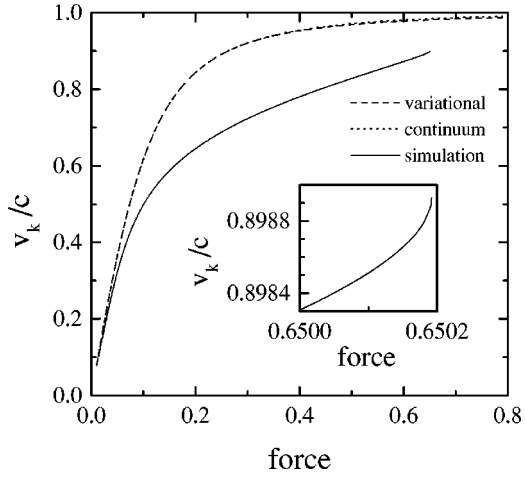

FIG. 1. The kink velocity v_k (normalized on the sound speed c) as a function of the driving force f for $g=1$, $\eta=0.1$, and $N=128$. The dashed curve corresponds to the SG dependence, Eq. (6), and the dotted curve, to the kink velocity in the continuum limit approximation.

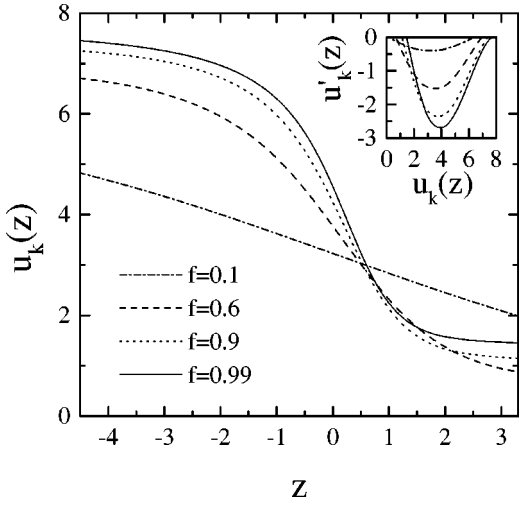

FIG. 2. Kink shape in the continuum limit approximation for $\eta=0.1$ and different values of the external force: $f=0.1$ (the dot–dashed curve), $f=0.6$ (the dashed curve), $f=0.9$ (the dotted curve), and $f=0.99$ (the solid curve). Inset: the separatrix of Eq. (8) for the same model parameters.

The kink solution corresponds to the boundary conditions $u_k(-\infty)=u_f+2\pi$, $u_k(+\infty)=u_f$, $u_k'(\pm\infty)=0$, or

$$w(u_f+2\pi)=w(u_f)=0, \tag{9}$$

where $u_f=\sin^{-1}f$. Close to the boundary points $\xi_0=u_f+2\pi$ or $\xi_0=u_f$ one can use the expansion $w(\xi)\approx w'(\xi_0)(\xi-\xi_0)$. Substituting this expansion into Eq. (8), we obtain

$$w'(u_f+2\pi)=(-\eta v+D)/2(c^2-v^2),$$
$$w'(u_f)=(-\eta v-D)/2(c^2-v^2), \tag{10}$$

where $D=[(\eta v)^2+4(c^2-v^2)\sqrt{1-f^2}]^{1/2}$. Thus, we have to look for a separatrix solution of Eq. (8), which satisfies the boundary conditions (9) and (10), that is possible for a given value of the parameter $v=v_k$ only. The dependence $v_k(f)$ obtained in this way for $\eta=0.1$ and $g=1$ (for other values of g one can rescale by introducing the dimensionless coordinate $\tilde{x}=x/\sqrt{g}$) is shown in Fig. 1 by the dashed curve. One can see that it practically coincides with the SG dependence, Eq. (6). Finally, the kink shape can then be restored from the function $w(\xi)$ by the integration

$$z=\int_{u_f+\pi}^{u_k(z)} d\xi\, w^{-1}(\xi). \tag{11}$$

The shape of the separatrix for different values of the external force f is presented as an inset in Fig. 2, and the corresponding shape of the kink, in Fig. 2. One can see that the shape of the driven kink is asymmetric at $f\neq 0$, the kink ''head'' is sharper, while its ''tail'' is more extended than those of the SG kink, as it directly follows from Eq. (10). It is indicated, however, that in the continuum limit approximation the kink shape is monotonic for all values of the driving force.

III. DISCRETE CHAIN: SIMULATION RESULTS

A. Automodel solution

To find the dependence $v_k(f)$ for the discrete FK chain, we started from the $f=0$ equilibrium state and slowly increased the force by small steps $\Delta f=10^{-3}$ with the rate 10^{-3}. After every step of changing the force, we looked for a steady-state solution of the motion equation (1) by the following method. First, we made the second-order Runge–Kutta (RK) iterations for a time $t'=2N\tilde{T}(f)$ with the time step $\Delta t=\tilde{T}(f)/M$, where N is the number of atoms (in the simulation we used $N=128,256,\ldots,2048$), M is an integer (we checked the results for $M=64$, 128, 512, 1024, and 8192), and $\tilde{T}$ is a parameter. At the beginning, i.e., at low forces $f<f_{\rm PN}$ when the kink does not move, we used the value $\tilde{T}=10$. We considered the kink as pinned if the velocity of the center of mass of the system averaged over the time t' $\langle v_{\rm cm}\rangle=\langle\Sigma_l\dot{u}_l(t')\rangle$, was lower than $10^{-4}c$. When the kink starts to move, i.e., at $f\geqslant f_{\rm PN}$, first we used the estimation of the delay time $\tilde{T}=2\pi/\langle v_{\rm cm}\rangle$ for the value of $\tilde{T}$. Then we started to vary $\tilde{T}$ and to test the value

$$\Delta U(\tilde{T})=\left(\sum_l \{[u_{l+1}(t+\tilde{T})-2\pi-u_l(t)]^2 + [\dot{u}_{l+1}(t+\tilde{T})-\dot{u}_l(t)]^2\}\right)^{1/2}, \tag{12}$$

looking for a minimum of the function $\Delta U(\tilde{T})$ for a given t. In more detail, we made iteration with $\tilde{T}_{n+1}=(1+\epsilon)\tilde{T}_n$ decreasing ϵ by two times at each step starting from $\epsilon=0.1$ and changing its sign if necessary in order to decrease the value ΔU at every step n. The iterations continued until $\epsilon\sim 10^{-15}$. In this way we found the steady-state solution for every value of f, which corresponds to a zero of the function, Eq. (12), with an accuracy $\Delta U<10^{-13}$, i.e., it satisfies the automodel condition

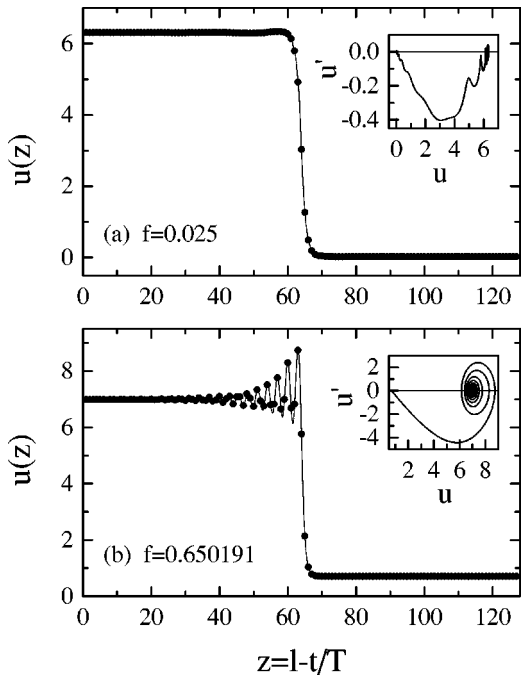

FIG. 3. Kink shape in the discrete chain as a function of $z=l-t/T(f)$ for: (a) a small force $f=0.025$ and (b) the critical force $f=0.650191$. $g=1$, $\eta=0.1$, $N=128$, and $M=64$. Black circles show instantaneous atomic positions and the solid curve corresponds to the ''automodel'' curve. Inset: the corresponding separatrices.

$$u_{l+1}(t)=u_l(t-T)+2\pi, \tag{13}$$

where $T=\tilde{T}_\infty$ is the delay time. The kink velocity is then determined as $v_k=2\pi/T$. The described algorithm allows us to calculate the dependence $v_k(f)$ with any desired accuracy (limited by accuracy of the RK method only, which is approximately the same for all values of the force due to the appropriate choice of Δt) and at the same time to test the automodel condition, Eq. (13), checking out whether the steady state is reached. Besides, this technique is faster than that used in [5,6], where the mean system velocity was calculated by averaging over long times. The algorithm with the fast Fourier transform [13] often used for such types of problems, also gives too slow convergence for the single kink problem.

To find the critical force $f_{\rm crit}$ when the moving kink becomes unstable, we also controlled the value $v_{\rm cm}$ at every RK step. When this value exceeds c, we returned back to the previously saved step of changing f, decreased Δf by ten times, and repeated the simulation. The procedure was continued untill the accuracy $\Delta f\sim 10^{-6}$ was reached.

The results of simulation for $g=1$ and $\eta=0.1$ are presented in Figs. 1, 3 and 4. First, the steady-state solution is automodel for *any* external force $f_{\rm PN}<f<f_{\rm crit}$. Second, the kink velocity in the discrete case is lower than that in the continuum limit approximation because of additional (intrinsic) damping of kink motion due to discreteness effects. Third, while in the continuum limit approximation the steady-state solution of moving kink exists for any force $f<1$; in the discrete chain such a solution exists only for $f<f_{\rm crit}$, where $f_{\rm crit}=0.650\,19$ for the parameters used in Fig. 1. At larger forces, $f>f_{\rm crit}$, the sharp transition to the running state takes place. The condition $f_{\rm crit}<1$ is satisfied and, therefore, the sharp transition to the running state exists only in the underdamped system, $\eta<\eta_{\rm max}$, when the kink can reach the critical velocity before the minima of the external potential disappear. For example, for $g=1$ we found that $\eta_{\rm max}=0.385\,7225$.

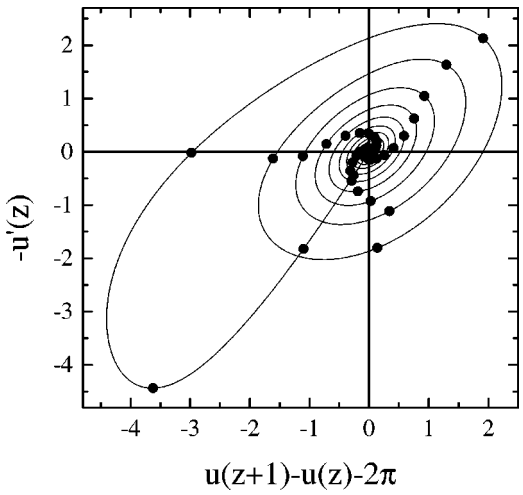

FIG. 4. Poincaré section $\dot{u}_l$ vs $u_{l+1}-u_l$. Black circles correspond to instantenious atomic coordinates and velocities. The parameters are the same as in Fig. 3(b).

The shape of running kink at different force values is shown in Fig. 3. These dependences can be presented as functions of one independent variable $z(f)=l-t/T(f)$, where l is the atomic index. Due to the automodel condition (13), the dependence $u_l(t)$ calculated for a time interval $0<t<NT$ for a given atom only, allows us to restore the evolution of all atoms in the chain, because each next atom repeats the trajectory of the previous atom in the chain with the delay time T. Note that in agreement with the continuum limit approximation, the discrete kink also has a sharp head and an extended tail, although the tail of the discrete moving kink has a complicated structure.

Comparing Figs. 2 and 3 one can see that, contrary to the

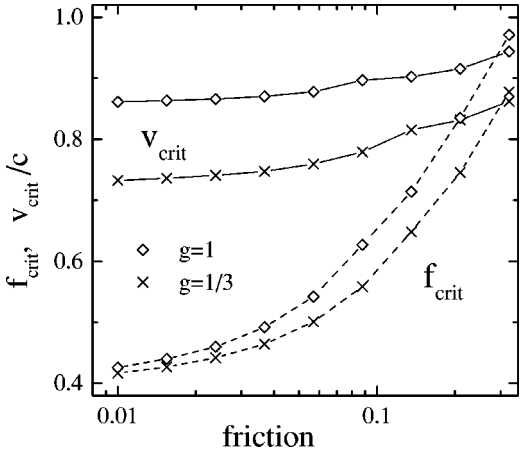

FIG. 5. The critical velocity $v_{\rm crit}/c$ (solid curves) and the critical force $f_{\rm crit}$ (dashed curves) as functions of the damping coefficient η for two values of the elastic constant: $g=1$ (diamonds) and $g=1/3$ (crosses). $N=256$.

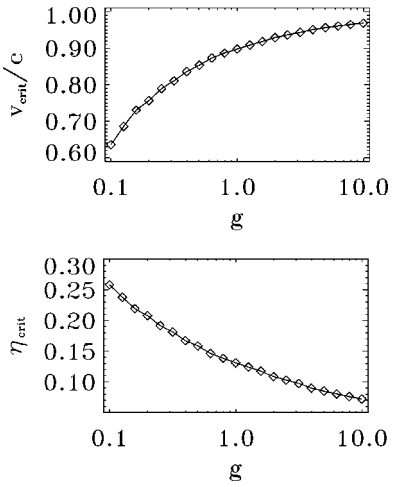

FIG. 6. The critical values v_{crit} and η_{crit} vs the elastic constant g for a fixed value of the external force $f=0.7$. $N=256$.

shape of a moving kink in the continuum limit approximation, the discrete kink has its own intrinsic structure. For example, the kink tail in Fig. 3(b) exhibits a spacial periodicity with a wave vector $k\approx 1/3$. The periodicity of the kink's tail is seen more clearly in Fig. 4, where we plot the velocities $\dot{u}_l(t)\propto -u'(z)$ versus the relative displacements $\Delta u(z)=u(z+1)-u(z)$ for all atoms for the interval $0<t<T$. For a given time t, such a picture corresponds to the stroboscopic map of the system. Recall that in the continuum limit approximation this dependence should be linear, because $\dot{u}(x,t)=-v_k u'(x,t)$ in this case.

B. Instability of fast kink

To understand a mechanism of instability of fast kinks, first we studied the dependence of critical values on system parameters. Figure 5 demostrates the critical kink velocity v_{crit} as a function of the external damping η for a fixed value of the elastic constant g. The instability exists only for the underdamped case, $\eta<\eta_{\max}$, when the kink can reach the critical velocity, which is close to the sound speed c, at some force $f_{\mathrm{crit}}<1$. At large frictions the maximum kink velocity is lower than c even in the $f\to 1$ limit, and the transition to the running state takes place at $f=1$ only, simply because the minima of the external potential disappear and all atoms go to the running state simultaneously.

In Fig. 6 we present the dependences of v_{crit} and η_{crit} on the discreteness parameter g for a fixed value of the external force $f=0.7$. In this simulation we used the following algorithm [14]. First, we prepared the initial configuration by relaxing the equidistant configuration at $f=0$ for a given value of g. Then we applied the dc force $f=0.7$ and allowed the system to reach a steady state, waiting a transient time $t_{\mathrm{tr}}=32\tau_0$. At the beginning, the external damping was taken to be large, $\eta=1$ (recall that the characteristic frequency of atomic vibration is $\omega_0=1$). After that we decreased the damping coefficient η with small steps (each new value of η was obtained from the previous one by dividing over 1.027 46, so we made 256 steps for changing η from $\eta=1$ to $\eta=10^{-3}$), and at each step we first waited for a time $32\tau_0$ to allow the system to reach a new steady state, and then for the next time period $t_{\mathrm{av}}=32\tau_0$ we measured the average system velocity. From these simulations one can see that the transi-

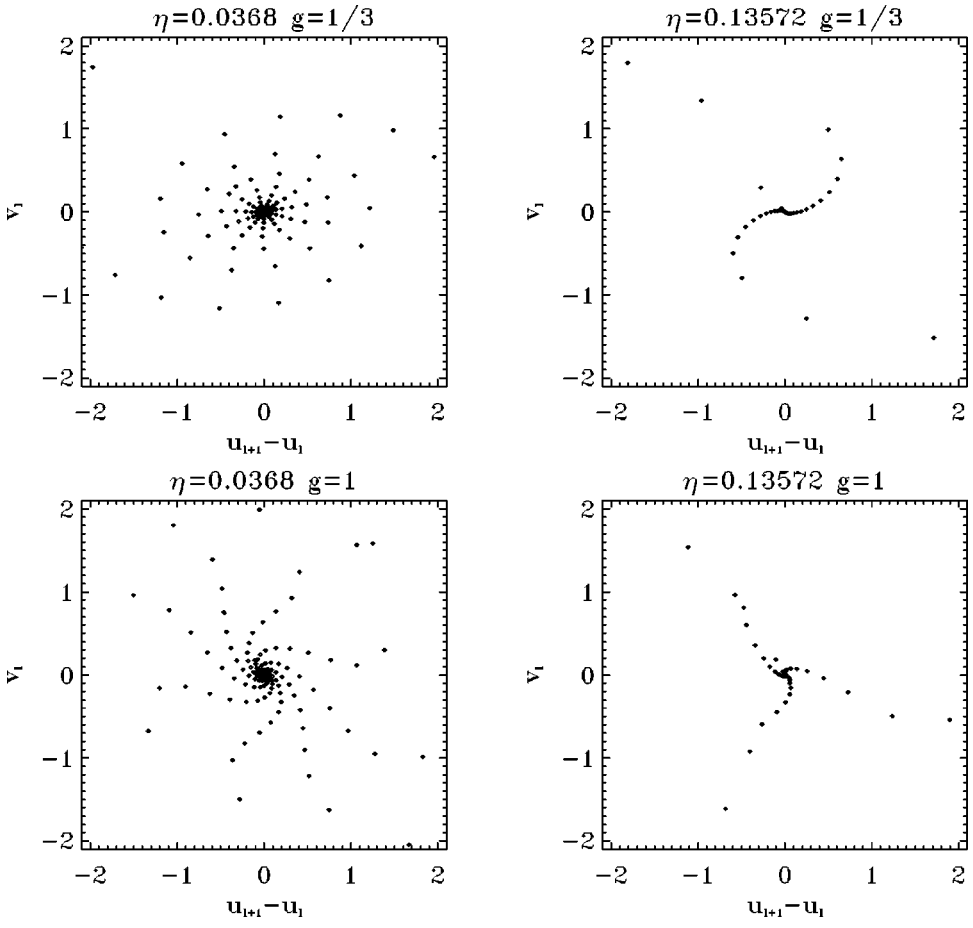

FIG. 7. Instantaneous system configuration (stroboscopic map) just before the kink destroying ($v_k\approx v_{\mathrm{crit}}$) for two different values of the damping coefficient ($\eta=0.036\,840$ and $\eta=0.135\,721$) and two values of the elastic constant ($g=1/3$ and $g=1$).

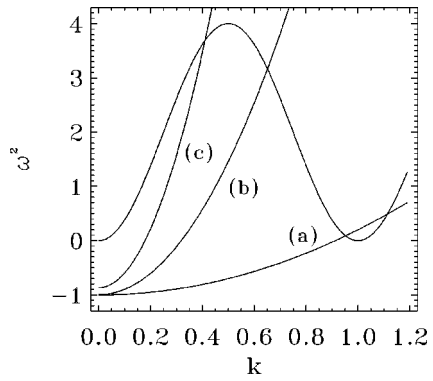

FIG. 8. Graphical solution of Eq. (14) in the extended Brillouin zone scheme for: (a) $f=0.025$, (b) $f=0.1$, and (c) $f=0.5$.

tion to the running state takes place when, due to the relativistic narrowing, the kink width $d_k=d(1-v^2/c^2)^{1/2}$ becomes small, $d_k<a$, so that the discreteness effects (oscillation of the moving kink in the PN potential) have to become too large.

In Fig. 7 we plot the stroboscopic map of the running kink for different values of the parameters g and η for the external force just before the kink is destroyed, when $v_k \to v_{\rm crit}(g,\eta)$. One can see that the kink tail at $f=f_{\rm crit}$ always demonstrates a periodic structure with relatively simple rational wave vectors like $k=1/2$, $k=1/3$, etc.

C. Kink's tail

The periodicity of the kink's tail may be explained similarly to the work of Peyrard and Kruskal [15]. In the frame comoving with the kink, the phonon spectrum is modified due to Doppler's effect, $\Omega_{\rm ph}(k)=\omega_{\rm ph}(k)-kv_k$. The kink may be followed by a standing wave (the wave comoving with the kink with the same phase velocity) if

$$\Omega_{\rm ph}(k)=0. \tag{14}$$

This equation always has one or more solutions as shown in Fig. 8 in the extended Brillouin zone scheme: $|k|<\infty$. At large kink velocities $v_k>2\omega_{\max}$, this solution corresponds to the wave vector within the first Brillouin zone [see curve (c) in Fig. 8]. At lower kink velocities the solution belongs to the second Brillouin zone [curve (b) in Fig. 8], then to the third Brillouin zone, etc. In the restricted Brillouin zone scheme, where $|k|<0.5$, we have to look for solutions of the equation $\Omega_{\rm ph}(k)=nv_k$, where $n=0,\pm1,\ldots$ is an integer. The graphical solution in this scheme is shown in Fig. 9. The solution with $n=0$ corresponds to the resonance of the washboard frequency $\omega_{\rm wash}=v_k$ with phonons, so the solutions with $n\neq1$ may be called ''super-resonances'' [7]. The dependence $k_{\rm res}(v_k)$ obtained by numerical solution of Eq. (14) is shown in Fig. 10. Note that at small kink velocities Eq. (14) has more than one solution. For example, for the case shown by curve (a) in Fig. 8, the lowest root corresponds to the oscillation behind the kink (the group velocity of phonons $v_{\rm gr}=d\omega_{\rm ph}(k)/dk$ is negative), and the second one to the oscillation ahead of the kink ($v_{\rm gr}>0$). Indeed, from Fig. 11 one can see that while at large velocity the kink shows oscillations in its tail only, at low velocities there are also oscillations ahead of the moving kink.

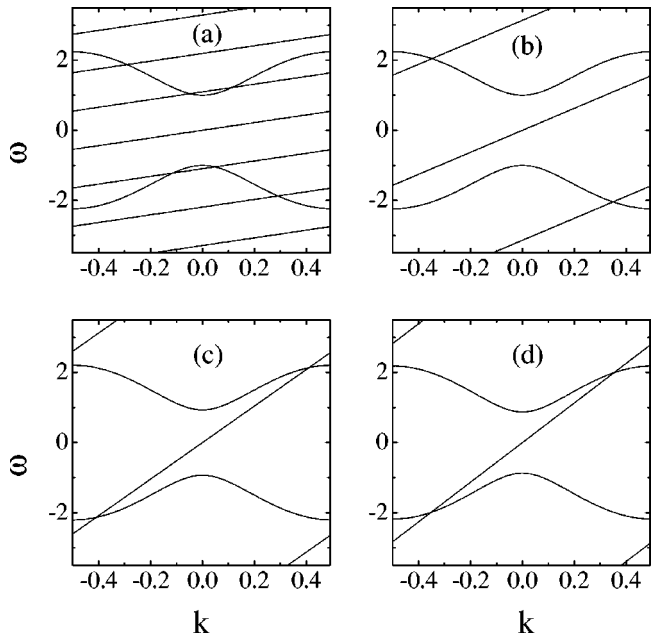

FIG. 9. Graphical solution of Eq. (14) in the restricted Brillouin zone scheme for: (a) $f=0.025$, $v_k=1.096$; (b) $f=0.1$, $v_k=3.133$; (c) $f=0.5$, $v_k=5.204$; and (d) $f=0.6502$, $v_k=5.648$.

To show that the described resonances are responsible for the tail's oscillation, we calculated the spacial Fourier transform of the kink shape

$$G(k)=T^{-1}\int_0^T dt\left|\sum_{l=1}^{N}\dot{u}_l(t)e^{i2\pi lk}\right|. \tag{15}$$

The function $G(k)$ is shown in Fig. 12. Then we found the maxima of $G(k)$ for different kink velocities and plotted their positions in Fig. 10. One can see that the short-wave component of kink tail oscillation is characterized by the wave vector which coincides with that obtained from the solution of Eq. (14) (see triangles in Fig. 10). In particular, for the force $f=0.65$, which is close to the critical force, we

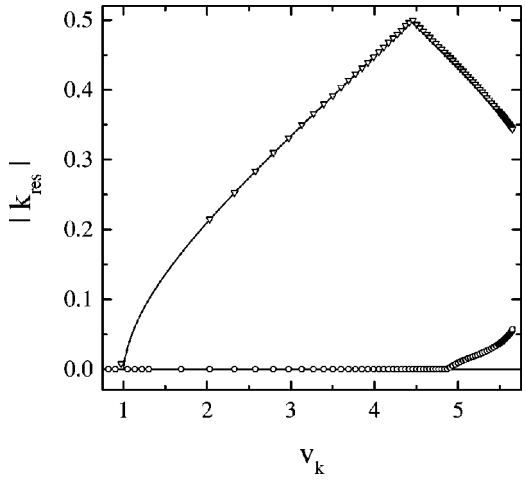

FIG. 10. The dependence $k_{\rm res}(v_k)$, where $k_{\rm res}$ is the solution of Eq. (14). Triangles and circles show the positions of maxima of the Fourier transform $G(k)$ of the kink's shape. The parameters are the same as in Fig. 1.

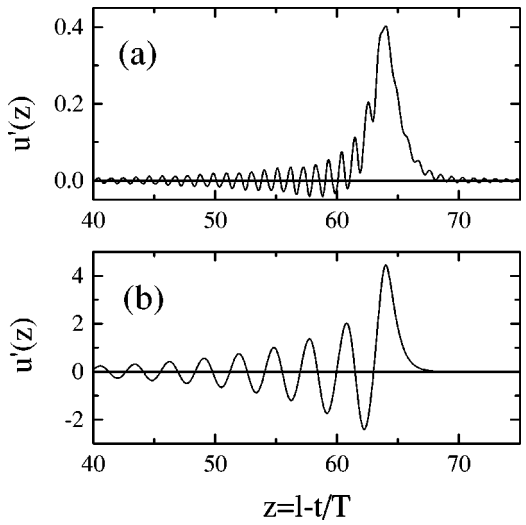

FIG. 11. Normalized atomic velocities $u'(z)=\dot{u}/T$ for the kinks shown in Fig. 3 for (a) $f=0.025$ and (b) $f=0.650\,191$.

obtained from Eq. (14) that $k\approx 1/3$ in agreement with periodicity of the kink's tail in Figs. 3(b) and 4.

To study the resonances in more details, we also calculated the response function $F(k,\omega)$ in the following way. We solved simultaneously the unperturbed motion equation (1) and the disturbed equation, where a small noise $\delta f_l(t)=\epsilon r_l(t)$, where $\epsilon=10^{-4}$ and $r_l(t)$ is a random number uniformly distributed within the interval $-1<r_l(t)<1$ was added to the external force f. Then we made the spatial–temporal Fourier transform of the difference of the disturbed and undisturbed solutions $F(k,\omega)$. [In fact, we simultaneously used six disturbed equations with different initializations of the random number generator and then averaged the calculated $F(k,\omega)$ values. Besides, to minimize a drift of the kink velocity due to noise, we orthogonalized the noise to the velocity vector $\{\dot{u}_l(t)\}$, $r_l(t)\to r_l(t)-\dot{u}_l(t)\Sigma_l[\dot{u}_l(t)r_l(t)]/\Sigma_l\dot{u}_l^2(t)]$. In Fig. 13 we plot $\ln|F(k,\omega)|$ as a gray scale map. Comparing these pictures with the restricted Brillouin zone (Fig. 9) we conclude that namely the excitation of phonons is responsible for the oscillating kink tail. However, Fig. 13 shows one more very important result: close to the critical velocity one can see from Fig. 13(c) and especially Fig. 13(d) that the resonance is spread. This indicates that just before the instability, the excitation becomes spatially localized.

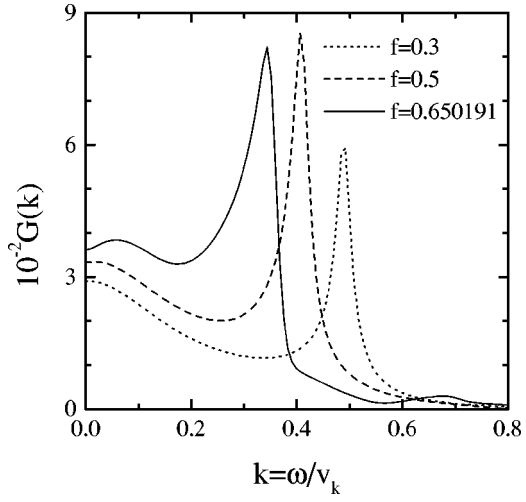

FIG. 12. Fourier transform $G(k)$ of the kink shape for $g=1$, $\eta=0.1$, and different forces: (a) $f=0.3$ ($v_k=4.543$), the dotted curve; (b) $f=0.5$ ($v_k=5.204$), the dashed curve; and (c) $f=0.650\,191$ ($v_k=5.648$), the solid curve.

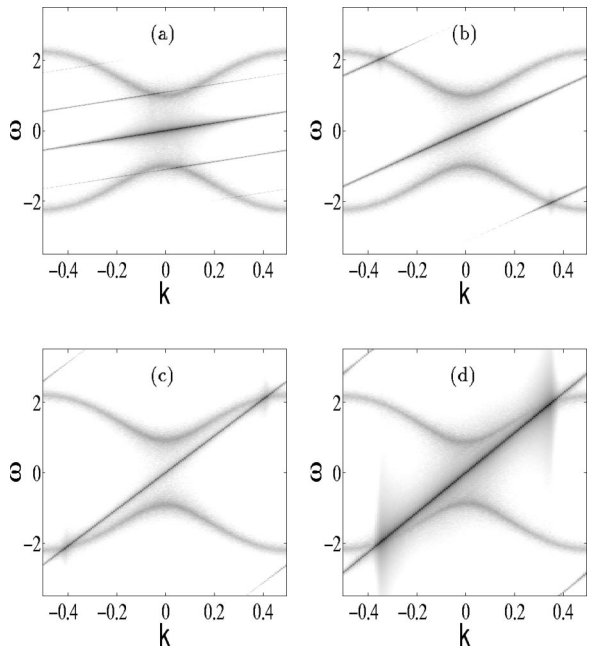

FIG. 13. The response function $F(k,\omega)$ as a gray scale map. $g=1$, $\eta=0.1$, $N=128$, and $M=64$, the force values in (a)–(d) are the same as in Fig. 9.

Another indication that the kink shape has a complicated structure just close to the critical velocity, follows from the Fourier transform, Eq. (15), of $\dot{u}_l(t)$. As can be seen from Fig. 12, close to $v_{\rm crit}$ the function $G(k)$ shows an additional peak corresponding to spatial oscillation of the tail with a small wave vector $k<0.1$ and frequency $\omega\ll\omega_{\rm min}$. This new branch is also shown in Fig. 10 by circles. We interpret these effects as an indication of the appearance of a shape mode (discrete breather) of the moving discrete kink just before it is destroyed. The same conclusion follows also from the Floquet analysis described in the next Sec. III D.

D. Floquet analysis

The motion equations (1) can be rewritten in a matrix form for the $2N$ vector $X\equiv\{x_l,\dot{x}_l\}$ as

$$\dot{X}=G(X). \tag{16}$$

Let $X_{\rm kink}(t)$ be the steady state (automodel) solution of Eq. (16), and let us look for a general solution in the form $X(t)=X_{\rm kink}(t)+Y(t)$, assuming $Y(t)$ to be small. Then $Y(t)$ has to satisfy the linearized equation

$$\dot{Y}(t)=B[X_{\rm kink}(t)]\,Y(t), \tag{17}$$

where $B(t)=\delta G/\delta X$. A formal solution of this equation is

$$Y(t)=C(t,0)\,Y(0), \tag{18}$$

where the matrix

$$C(t,0)=\exp\int_0^t dt\,B(t) \tag{19}$$

corresponds to the *time-ordered* matrix exponent which is defined as the limit of product

$$\exp(\Delta t\,B_M)\exp(\Delta t\,B_{M-1})\ldots\exp(\Delta t\,B_1), \tag{20}$$

where $B_k=B(k\,\Delta t)$, $\Delta t=T/M$, and the limit $M\to\infty$ is assumed.

Calculation of the expression (20) is connected with a large number of matrix multiplications. Instead, from Eq. (19) one can derive the differential equation for the matrix $C(t,0)$

$$\dot{C}(t,0)=B(t)\,C(t,0),\quad C(0,0)=J, \tag{21}$$

where J is the $2N\times 2N$ identity matrix, and then to solve Eq. (21) with the RK method. This procedure is about ten times faster than that with the exponents' multiplication. To simplify the calculation, we also used the substitution

$$Y(t)=\tilde{Y}(t)\exp(-\eta t/2), \tag{22}$$

so that Eq. (21) takes the form

$$\frac{d}{dt}\tilde{C}(t,0)=\tilde{B}(t)\,\tilde{C}(t,0),\quad \tilde{C}(0,0)=J, \tag{23}$$

where $\tilde{C}(t,0)=C(t,0)\exp(\eta t/2)$, and the matrix $\tilde{B}(t)$ has the form

$$\tilde{B}(t)=\begin{pmatrix}0 & I\\ A(t) & 0\end{pmatrix}, \tag{24}$$

where I is the $N\times N$ identity matrix, and the matrix $A(t)$ is defined by

$$A(t)=\begin{pmatrix}a_1(t) & 1 & 0 & \ldots & 0 & 1\\ 1 & a_2(t) & 1 & \ldots & 0 & 0\\ 0 & 1 & a_3(t) & \ldots & 0 & 0\\ \vdots & \vdots & \vdots & \ddots & \vdots & \vdots\\ 1 & 0 & 0 & \ldots & 1 & a_N(t)\end{pmatrix} \tag{25}$$

with $a_l(t)=-2-\cos x_l^{\rm kink}(t)+(\eta/2)^2$.

The Floquet technique deals with the stability of time periodic solutions. In the model with periodic boundary conditions we have to choose the time NT as the period of kink motion along the whole system. Integration of Eq. (23) over the period NT determines the Floquet matrix $\tilde{C}(NT,0)$ which linearly relates $\tilde{Y}(NT)$ to its initial value $\tilde{Y}(0)$. Then, we have to solve the corresponding eigenproblem,

$$\tilde{C}(NT,0)\,\tilde{Y}=\tilde{\lambda}\,\tilde{Y}. \tag{26}$$

The time NT in Eq. (26) can be reduced to T with the help of the automodel condition (13) of the steady-state solution. Indeed, taking into account the automodel condition, one can write

$$A(t+T)=p\,A(t)\,p^{-1}, \tag{27}$$

where p is the cyclic shift matrix

$$p=\begin{pmatrix}0 & 0 & \ldots & 0 & 1\\ 1 & 0 & \ldots & 0 & 0\\ 0 & 1 & \ldots & 0 & 0\\ \vdots & \vdots & \ddots & \vdots & \vdots\\ 0 & 0 & \ldots & 1 & 0\end{pmatrix}. \tag{28}$$

The matrix $\tilde{C}$ is transformed correspondingly as

$$\tilde{C}(t+T,0)=P\,\tilde{C}(t,0)\,P^{-1}, \tag{29}$$

where P is the block matrix

$$P=\begin{pmatrix}p & 0\\ 0 & p\end{pmatrix}. \tag{30}$$

So, we have

$$\tilde{C}(NT,0)=\tilde{C}[NT,(N-1)T]\times\tilde{C}[(N-1)T,(N-2)T]\ldots\tilde{C}(T,0), \tag{31}$$

or by using $P^N=I$, owing to periodic boundary conditions, we finally obtain

$$\tilde{C}(NT,0)=[P^{-1}\tilde{C}(T,0)]^N. \tag{32}$$

Thus, we can use the matrix $S(T)=P^{-1}\tilde{C}(T,0)$ and look for a solution to the eigenvalue problem $S(T)\tilde{Y}=\mu\tilde{Y}$. Then $\tilde{\lambda}=\mu^N$, and finally the eigenvalues of the primary matrix $C(NT,0)$ are $\lambda=\tilde{\lambda}\exp(-\eta t/2)$. Note that the substitution, Eq. (22), does not affect the eigenvectors of the problem.

The procedure described above was performed for different time steps of the RK method $\Delta t=T/M$ with $M=64,128,\ldots,8192$ for the chain of $N=128$ atoms. We determined the dependence of the accuracy of the solution of the eigenvalue problem on the accuracy of calculation of the steady-state kink shape using, as the test condition, the fact that for the exact solution one of the eigenvalues must be equal to $\lambda_1=1$, and the corresponding eigenvector must be proportional to $\dot{X}_{\rm kink}(t)$. We found that decreasing the time step Δt leads to some improvement of the results (for example, $|\lambda_1-1|\sim 10^{-4}$ for $M=64$ and $|\lambda_1-1|\sim 10^{-10}$ for $M=8192$, correspondingly), but the qualitative picture remains unchanged, so in order to reduce the computational time we performed most of calculations with $M=64$.

The results of the calculation are the following (see Figs. 14–16):

(1) All eigenvalues λ lie symmetrically with respect to the circle of radius $R=\exp(-\eta T/2)$ (recall that T depends on the force f) and have properties similar to those for the Hamiltonian problem, where the corresponding Floquet matrix is

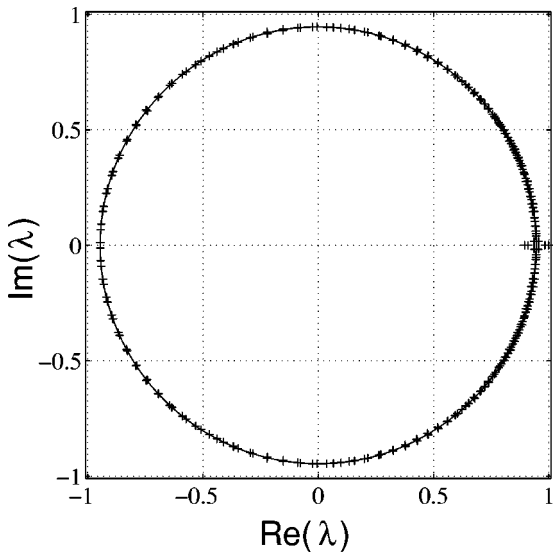

FIG. 14. Floquet eigenvalues for $g=1$, $\eta=0.1$, $f=0.65$, $N=128$, and $M=64$. The circle corresponds to $R=\exp(-\eta T/2)$.

symplectic. Namely, we determined that if λ is an eigenvalue, then λ^*, R^2/λ, and R^2/λ^* are also eigenvalues with the same numerical accuracy.

(2) The two eigenvalues are always real, $\lambda_1=1$ [this trivial solution corresponds to the translational, or phase mode with the eigenvector $Y_1(t)\propto\dot{X}_{\rm kink}(t)$] and, symmetrically to it, $\lambda_1'=\exp(-\eta T)$. Note that for time-reversible (e.g., Hamiltonian) systems these eigenmodes are twice degenerated and both correspond to the $\lambda=1$ eigenvalue (e.g., see [16]).

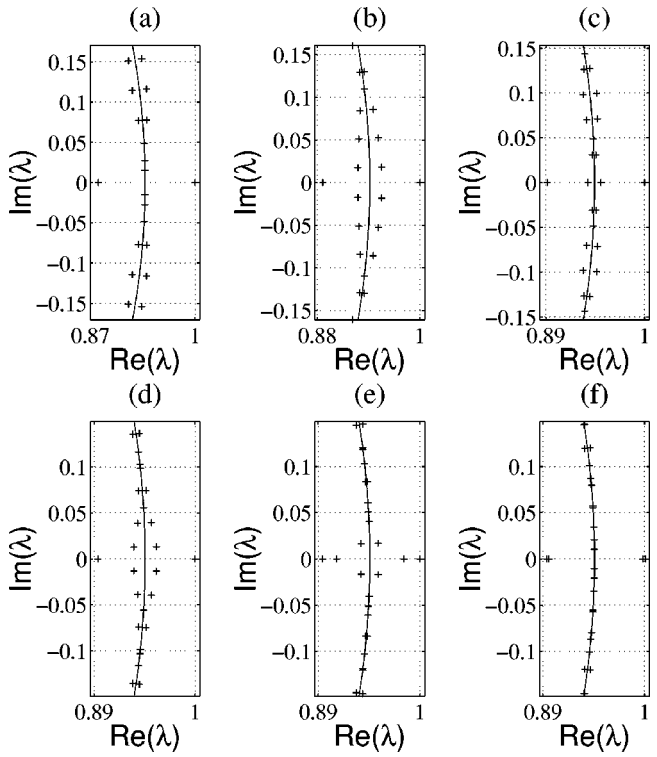

FIG. 15. Evolution of the Floquet eigenvalues with f changing: (a) $f=0.4$, (b) $f=0.5$, (c) $f=0.6$, (d) $f=0.645$, (e) $f=0.65$, and (f) $f=0.650\,191$.

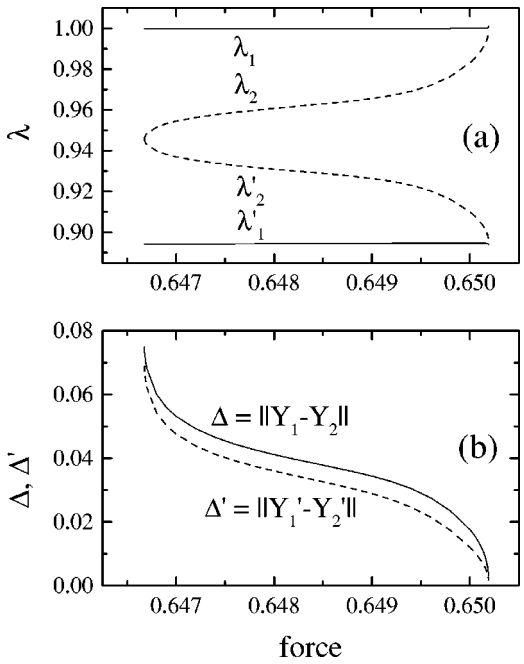

FIG. 16. Dependence of eigenvalues and eigenvectors on the force f: (a) the eigenvalues λ_1, λ_1', λ_2, and λ_2', and (b) the distance between the corresponding eigenvectors $\Delta=||\tilde{Y}_1-\tilde{Y}_2||=\{(2N)^{-1}\Sigma_{l=1}^{2N}[(\tilde{Y}_1)_l-(\tilde{Y}_2)_l]^2\}^{1/2}$ and $\Delta'=||\tilde{Y}_1'-\tilde{Y}_2'||$.

(3) At small forces, $f\ll f_{\rm crit}$, all other eigenvalues lie on the circle R. With the increase of f some of eigenvalues may ''collide'' and go out of the circle, probably due to parametric resonances, but then they come back to the circle. Because the eigenvalues do not go outside of the $R=1$ circle, this effect does not lead to an instability as it does in Hamiltonian systems.

(4) At high forces close to $f_{\rm crit}$ (namely, for $f>0.646\,676\,04$ for the chosen set of parameters), another pair of eigenvalues λ_2 and λ_2' become real and leave the $R=\exp(-\eta T/2)$ circle as is demonstrated in Fig. 15. At $f\to f_{\rm crit}$ this second pair approaches the first one, $\lambda_2\to\lambda_1$ and $\lambda_2'\to\lambda_1'$ (see Fig. 16). The corresponding eigenvectors also tend to one another. A general Floquet theory states that when two eigenmodes coincide having the $\lambda=1$ eigenvalue, the corresponding steady state of the system becomes unstable (e.g., see [17], Chap. I, theorem 3.2).

Evolution of the eigenvalues λ_2 and λ_2' and the corresponding eigenvectors $\tilde{Y}_2$ and $\tilde{Y}_2'$ with changing dc force f is presented in Figs. 16 and 17. One can see that at the beginning, when the λ_2 mode just emerges [Fig. 17(a)], it corresponds to an almost pure phononic (nonlocalized) mode, but with increasing f the degree of its localization increases. Thus, the λ_2' mode can be considered as the discrete breather solution excited by the moving kink. From the inset in Fig. 1 one can see also that just before $f_{\rm crit}$ the kink velocity sharply increases, d^2v_k/df^2 changes its sign, and dv_k/df tends to infinity at $f\to f_{\rm crit}$ ($dv_k/df\approx 10.5$ at $f=0.65$ and $dv_k/df\approx 2.89\times 10^3$ at $f=0.650\,19$).

E. Kinetics after kink destroying

To study the scenario of kink destroying in details, we started from the steady state corresponding to the kink mo-

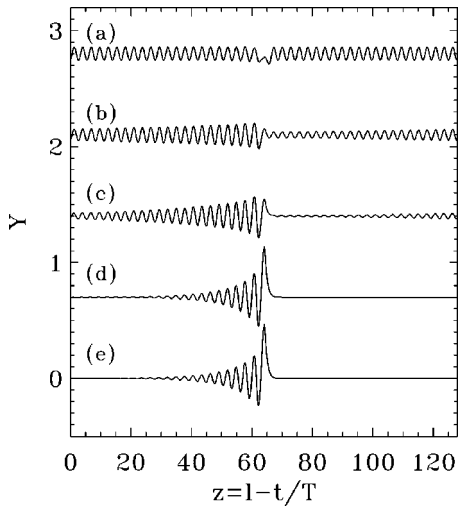

FIG. 17. The eigenvector $\tilde{Y}_2$ for different force values: (a) $f=0.646\,676\,04$, (b) $f=0.6468$, (c) $f=0.648$, and (d) $f=0.650\,191\,9086$. (e) shows the eigenvector $\tilde{Y}_1$ for $f=0.650\,191\,9086$; note that it looks practically the same for all forces used in the present figure. The curves were obtained as the solutions of linearized motion equation with initial condition corresponding to the eigenvector Y_2 so they may be treated as atomic trajectories corresponding to the λ_2 eigenmode. The $\tilde{Y}_2$ curves are artificially shifted upstairs to be shown all in one figure.

tion with $v_k \approx v_{\text{crit}}$ ($f=0.65$ for the parameters $g=1$ and $\eta=0.1$) and then slightly increased the force (to the value $f=0.651$). The results of simulation are presented in Fig. 18, where we plot $u_l(t)$ versus the index l for different time moments, each next curve being slightly shifted upstairs and to the right. One can see that the scenario is the following. The first event is the creation of a new kink-antikink pair in the tail of the primary kink. The newly created antikink moves to the left, while the primary kink and the newly created kink produce the ''double'' kink which moves as a whole. Then one more kink-antikink pair is created in the tail of the double kink; again the second antikink moves to the left, while the new kink plus the double kink produce the

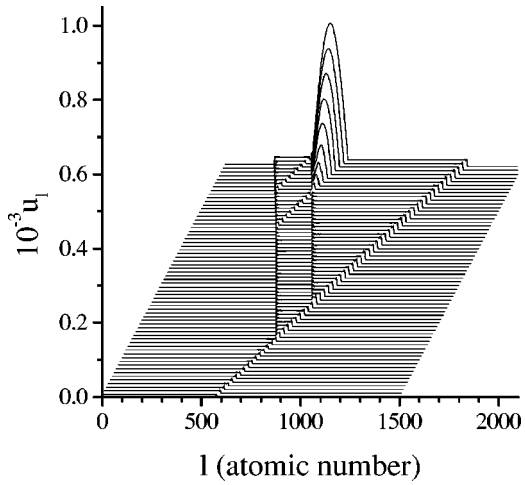

FIG. 18. Evolution of the system at $f=0.651$ starting from the initial state corresponding to the steady state for $f=0.65$, when $v_k \approx v_{\text{crit}}$. The system parameters are $g=1$, $\eta=0.1$, and $N=1500$.

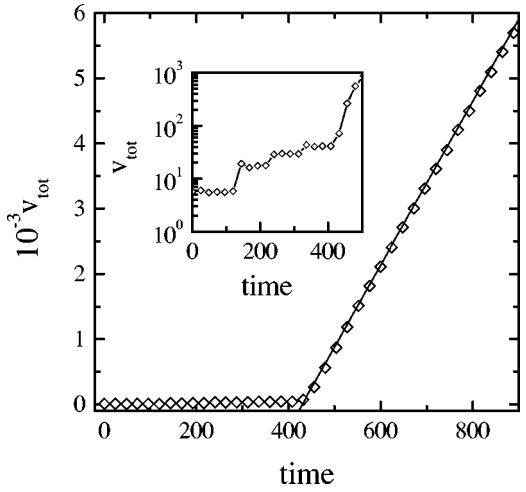

FIG. 19. The dependence $v_{\text{tot}}(t)$ for the system evolution at $f=0.651$. The solid line describes the fit $v_{\text{tot}}(t)=2c(t-t_0)$. Inset: the same in the logarithmic scale. Parameters are as in Fig. 18.

''triple'' kink. Then, the first *antikink* creates behind itself one more kink–antikink pair. The kink from this last created pair moves to the right and finally meets with the second antikink. After their collision an avalanche starts to grow.

Figure 19 shows the evolution of the total system velocity $v_{\text{tot}}(t)=\Sigma_l \dot{u}_l(t)$ during this process. When the first kink–antikink pair is created, v_{tot} increases two times (see details in inset of Fig. 19), then it again increases at the next creation events, and finally, when the avalanche starts to grow, v_{tot} begins to increase linearly with time with the velocity $2c$, so that both fronts of the running domain move with the sound speed.

Figure 20 demonstrates the shape of the growing domain of running atoms. In this figure we plot the function $\rho_l(t)$

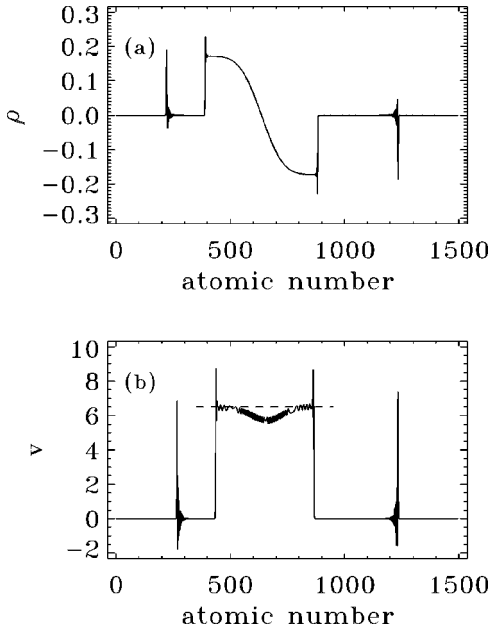

FIG. 20. Structure of the running domain at a fixed time moment: (a) the density of excessive atoms $\rho_l(t)=-[u_{l+1}(t)-u_l(t)]/(2\pi)^2$ and (b) the atomic velocities $v_l(t)$. Parameters are as in Fig. 18.

$=-[u_{l+1}(t)-u_l(t)]/(2\pi)^2$, which describes the density of excessive atoms in comparison with the commensurate structure, and the atomic velocities $\dot{u}_l(t)$ for a fixed time moment. One can see that in the running domain the atomic velocities are almost constant and are approximately equal to the maximum atomic velocity $f/\eta=6.5$, and that ahead of the fronts of the running domain, one can see the running triple kink and the double antikink.

The shape of the function $\rho(x,t)$ in the running domain may be explained in the following way. Differentiating Eq. (3) over x, we obtain for the function $\rho(x,t)=-u'(x,t)/2\pi$ the following equation:

$$\ddot{\rho}+\eta\dot{\rho}-\rho''+[\cos u(x,t)]\,\rho=0. \tag{33}$$

Averaging this equation over time for a period T, we obtain for a slowly varying component of the density the following equation:

$$\overline{\rho}''(x)+k_r^2\overline{\rho}(x)=0, \tag{34}$$

where $k_r^2=-\langle\cos u(x,t)\rangle$ and $0<k_r^2\ll 1$. Thus, in the running domain $\overline{\rho}(x)\propto\sin k_r(x-x_c)$, where x_c is the center of the running domain.

IV. CONCLUSION

Thus, we have studied the underdamped driven dynamics of topological excitations (kinks) in the discrete SG chain and showed that the steady-state kink motion is always automodel, each atom repeats the trajectory of the previous atom with the time delay $T=2\pi/v_k$. The shape of moving kink is asymmetric, has a sharp head, and an extended oscillating tail. Due to discreteness effects the kink tail has a complicated intrinsic structure, and it shows spacial oscillations with the wave vector k defined by the resonance of the washboard frequency $\omega=v_k$ with phonons.

At a large force, a localized shape mode (discrete breather) emerges in the kink tail. With increasing kink velocity, the amplitude of this excitation increases too, and at some critical velocity the DB decays into the kink–antikink pair. This instability exists only in the underdamped system, $\eta<\eta_{\max}<0.5$, when the kink can reach the critical velocity at a force lower than $f=1$. In the overdamped system the kink velocity remains lower than the critical one even in the $f\to 1$ limit, so the sharp transition cannot emerge.

The emission of kink-antikink pairs in the tail of the fast kink leads to the sharp transition to the running state just after the first collision of the secondary kink and antikink. At the collision, the atoms in the collision region go to the running state, and this running domain then grows with the sound speed. Atoms in the running domain have velocities close to the maximal value, while the atomic density has a cosine profile. Besides, we observed that the double and triple fast kinks in the front of the running domain remain stable, at least on the time scale of our simulation.

Although most of the simulation presented in the paper was performed for given parameters of the system ($g=1$ and $\eta=0.1$), we determined that the described scenario remains the same for other parameters as well. Thus, we conclude that the scenario described in the present work (i.e., the excitation of the discrete breather in the tail of the fast moving topological excitation, the decay of this DB into a pair of new topological excitations, then their collision with the subsequent growing of the running domain) should be generic for a wide class of nonlinear systems.

ACKNOWLEDGMENTS

We gratefully acknowledge helpful discussions with S. Aubry, A. R. Bishop, and M. Peyrard. This work was supported in part by grants from Hong Kong Research Grants Council (RGC) and Hong Kong Baptist University (FGR). O.B. was partially supported by NATO Grant No. HTECH.LG 971372 and INTAS Grant No. 97-31061.

[1] B. N. J. Persson, *Sliding Friction: Physical Principles and Applications* (Springer, Berlin, 1998).
[2] O. M. Braun, T. Dauxois, and M. Peyrard, Phys. Rev. B **56**, 4987 (1997).
[3] B. N. J. Persson, Phys. Rev. Lett. **71**, 1212 (1993); Phys. Rev. B **48**, 18 140 (1993).
[4] O. M. Braun, T. Dauxois, M. V. Paliy, M. Peyrard, and B. Hu, Physica D **123**, 357 (1998).
[5] O. M. Braun, T. Dauxois, M. V. Paliy, and M. Peyrard, Phys. Rev. Lett. **78**, 1295 (1997); Phys. Rev. E **55**, 3598 (1997); M. Paliy, O. Braun, T. Dauxois, and B. Hu, *ibid.* **56**, 4025 (1997).
[6] O. M. Braun, A. R. Bishop, and J. Röder, Phys. Rev. Lett. **79**, 3692 (1997).
[7] F.-J. Elmer, Phys. Rev. E **50**, 4470 (1994); M. Weiss and F.-J. Elmer, Phys. Rev. B **53**, 7539 (1996).
[8] M. G. Rozman, M. Urbakh, and J. Klafter, Phys. Rev. Lett. **77**, 683 (1996); Phys. Rev. E **54**, 6485 (1996); Europhys. Lett. **39**, 183 (1997).
[9] O. M. Braun and Yu. S. Kivshar, Phys. Rep. **306**, 1 (1998).
[10] O. M. Braun, Yu. S. Kivshar, and M. Peyrard, Phys. Rev. E **56**, 6050 (1997).
[11] F. Zhang, Phys. Rev. E **54**, 4325 (1996).
[12] J.-A. Sepulchre and R. S. MacKay, Physica D **113**, 342 (1998).
[13] T. Strunz and F.-J. Elmer, Phys. Rev. E **58**, 1601 (1998).
[14] O. M. Braun, B. Hu, A. Filippov, and A. Zeltser, Phys. Rev. E **58**, 1311 (1998).
[15] M. Peyrard and M. D. Kruskal, Physica D **14**, 88 (1984).
[16] S. Aubry, Physica D **103**, 201 (1997).
[17] J. K. Hale, *Oscillators in Nonlinear Systems* (McGraw-Hill, New York, 1963).